15

Ultrafast Coherent Spectroscopy of Single Semiconductor Quantum Dots

Christoph Lienau and Thomas Elsaesser

Abstract. This chapter summarizes our recent work—performed within the project B6 of the Sonderforschungsbereich 296—on combining ultrafast spectroscopy and near-field microscopy to probe the nonlinear optical response of a single quantum dot and of a pair of dipole-coupled quantum dots on a femtosecond time scale. We demonstrate coherent control of both amplitude and phase of the coherent quantum dot polarization by studying Rabi oscillations and the optical Stark effect in an individual interface quantum dot. By probing Rabi oscillations in a pair of laterally coupled interface quantum dots, we identify couplings between excitonic dipole moments and reveal the microscopic origin of these couplings. Our results show that although semiconductor quantum dots resemble in many respects atomic systems, Coulomb many-body interactions can contribute significantly to their optical nonlinearities on ultrashort time scales. This is important for realizing potentially scalable nonlocal quantum gates in chains of dipole-coupled dots, but also means that decoherence phenomena induced by many-body interactions need to be carefully controlled.

15.1 Introduction

The experimental implementation of quantum information processing (QIP) relies on identifying, coherently manipulating, coupling and detecting elementary excitations of individual quantum systems. All these operations need to be performed on a time scale much shorter than the decoherence time of the quantum system. This extremely challenging task has attracted the interest of an increasing number of researchers in all areas of science. Implementations of quantum logic operations are currently explored in a wide range of different quantum systems [1], e.g., nuclear magnetic spins in liquids and solids [2, 3], ions in traps [4–7], atoms in microwave resonators [8], optical lattices [9], photonic band gap materials [10], Josephson junctions [11, 12] or photons in quantum-optical systems [13, 14]. The complexity of this endeavor is quite clearly demonstrated by the fact that, despite the outstanding progress in this

field over the last few years, the most complex quantum calculation performed to date is the factorization of the number 15 [3].

A particularly attractive approach to realizing all-solid-state quantum information processing relies on using charge or spin excitations of semiconductor quantum dots (QDs) as quantum bits. In QDs, electron and hole wave functions are localized in all three spatial dimensions on a nanometer length scale due to growth-induced nanoscale variations of the semiconductor composition. This makes QDs interesting model systems for exploring the basic physics of quasi-zero-dimensional quantum confinement as well as interesting for building novel optical devices for information processing.

The optical and electronic properties of semiconductor QDs have been intensely studied during the last decade. Due to the pronounced and so far unavoidable growth-induced inhomogeneous broadening in ensembles of semiconductor QDs, the recent development of single QD spectroscopy has provided a wealth of new information [15]. It is now understood that sufficiently confined QDs resemble in many respects atomic systems, showing atomic-like densities of states [16–18], a shell-like absorption spectrum [19] and—at low temperatures—comparatively long dephasing times of up to 1 ns [20, 21]. In addition, the nanometer spatial extent of the electron wave function in QDs gives rise to excitonic dipole moments of 10–100 Debye, much larger than those of atomic systems. This strong coupling to light makes charge excitations of single quantum bits interesting for quantum information processing. Ultrafast light pulses with pulse durations in the 100-fs range allow for generating and manipulating exciton excitations of single QDs on a subpicosecond time scale. With such ultrafast coherent carrier control, dephasing times in the 100-ps to 1-ns range are comparably long, making in principle up to 10,000 coherent manipulations possible before decoherence destroys the quantum information stored in excitonic quantum bits [21]. Another important consequence of the large excitonic dipole moments are comparatively strong dipolar interactions between adjacent quantum dots [22, 23]. Those interactions give rise to a nonlocal coupling between adjacent excitonic quantum bits, an important prerequisite for implementing scalable quantum gates. Consequently, different ideas for realizations of such gates have been proposed theoretically in recent years [22–25].

Such perspectives have triggered a research effort toward coherent control of excitonic excitations in semiconductor quantum dots. Initial successful experiments have shown coherent control on excited state transitions in the weak excitation regime [26–28] before Rabi oscillations could be demonstrated on different quantum dot systems [29–33]. All these experiments have so far revealed a finite damping of Rabi oscillations, which has been attributed either to excitation-induced dephasing due to Coulomb interactions among charge excitations [29, 34] or to exciton–phonon coupling [35, 36]. Most recently, an all-optical two-bit quantum logic gate was demonstrated using the exciton and biexciton transitions of a single quantum dot [37].

Here we present our recent experimental work on coherent control of excitonic excitations in quantum dots. We discuss a novel nano-optical technique [34] for probing optical nonlinearities of single quantum dots on ultrafast time scales [34, 38]. Coherent control of both amplitude [39] and phase [40] of the coherent exciton po-

larization in a single interface quantum dot is demonstrated and interactions between permanent excitonic dipole moments in a pair of neighboring quantum dots are resolved by analyzing Rabi oscillations in their nonlinear optical response [39].

In Sect. 15.2 we summarize the relevant properties of the investigated samples. In Sect. 15.3 we describe our experimental techniques. Results on coherent control of single quantum dots are given and discussed in Sect. 15.4. In Sect. 15.5 we present first results on dipolar couplings between two quantum dots. In Sect. 15.6 we give some conclusions.

15.2 Interface Quantum Dots

An important QD model system are thin semiconductor quantum wells (QWs). In quantum wells, local monolayer height fluctuations at the interfaces (interface roughness) and fluctuations of the alloy composition (alloy disorder) are unavoidable (Fig. 15.1(a)). The resulting disordered potential leads to the localization of excitons in single "interface" QDs with a confinement energy of about 10 meV (Fig. 15.1(b)). This disorder gives rise to a pronounced inhomogeneous broadening of far-field optical spectra. In experiments with high spatial and spectral resolution, however, the smooth, inhomogeneously broadened photoluminescence (PL) spectra break up into narrow emission spikes from a few localized excitons [16–18, 41–43].

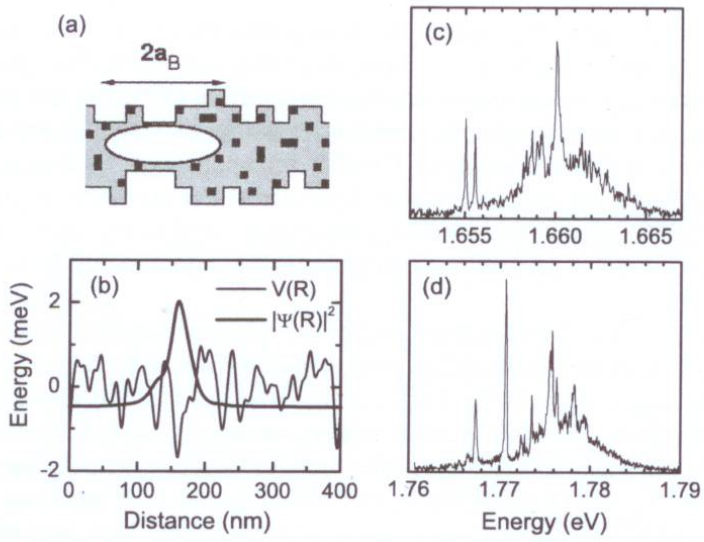

Fig. 15.1. (**a**) Disorder in quantum wells arises from spatial fluctuations of the local quantum well thickness (interface roughness) and of the quantum well composition (alloy disorder). (**b**) Schematic illustration of the effective disorder potential $V(\boldsymbol{R})$ and of a localized excitonic center-of-mass wave function $|\Psi(\boldsymbol{R})|^2$. (**c**)–(**d**) Representative near-field PL spectra (T = 12 K) of (**c**) a 5.1 nm thick and (**d**) a 3.3 nm thick (100) GaAs QW

The linear optical properties of interface QDs resemble in many aspects those of atomic systems. At low temperatures, the excitonic lines display a narrow homogeneous line width of 30–50 μeV, in agreement with measured dephasing times of 20–30 ps. The QDs show a discrete absorption spectrum [18] and often a fine structure splitting due to the spatial asymmetry of the monolayer islands. The temperature dependence of the exciton line width and the fine structure splitting has been thoroughly investigated [18, 44]. The correlation length of the disordered potential and thus also the center-of-mass wave function of localized excitons in QDs typically extends over several tens of nm, as known from near-field autocorrelation spectroscopy [42]. This large extension of the excitonic wave function results in large QD dipole moments of 50–100 Debye and a particularly strong coupling of these excitons to light [45, 46]. This makes interface QDs a particularly interesting model system for nonlinear spectroscopy of single QDs.

In this work, we investigate a sample consisting of 12 single QW layers of different thicknesses grown on a (100) GaAs substrate. The QW layers are separated by AlAs/GaAs short-period superlattice barriers, each formed by nine AlAs and GaAs layers with a total thickness of 23.8 nm. Here, we study the top seven QWs with thicknesses of 3.3–7.1 nm. The layers are buried at distances between 40 and 211 nm below the surface. Growth interruptions of 10 s at each interface lead to a large correlation length of the QW disorder potential and to the formation of interface QDs. The growth interruptions are kept short in order to avoid a monolayer splitting of the macroscopic PL spectra and to minimize the incorporation of impurities at the interfaces.

In Fig. 15.1(c) and (d) representative low temperature ($T = 12$ K) near-field PL spectra are shown for the 3.3 and 5.1 nm thick (100) GaAs QW. The spectra clearly reveal the emission from excitons localized in interface QDs. The line width of the sharp resonances is limited by the spectral resolution of 100 μeV. The spectra are recorded at an excitation intensity of 110 nW, corresponding to an average excitation density well below one exciton per monolayer island. For excitation powers between 1 and 500 nW, we find a linear intensity dependence and an excitation-independent shape of the emission spectra, indicating negligible contributions from biexcitons and charged excitons.

In addition to the sharp localized exciton emission, at higher energies these spectra display a spectrally broad background emission from more delocalized excitons in QW continuum states [42]. This is a disadvantage for QIP applications, as it may be difficult to avoid the uncontrolled population of such delocalized exciton states when ultrashort and thus spectrally broadband pulses are used for optical excitation. Yet, we will demonstrate in the following that such problems can be reduced by careful spectral shaping of the excitation pulses. Important properties of interface QDs are the excellent interface quality of the (100) GaAs quantum wells and the strong reduction of piezoelectric and strain fields. In the investigated samples, the energetic positions of the sharp exciton emission lines remains unchanged over many hours and we observe no signs of a spectral diffusion of the exciton lines.

15.3 Coherent Spectroscopy of Interface Quantum Dots: Experimental Technique

In the experiments on interface QDs, we read out quantum information from a single QD by directly probing the transient nonlinear optical spectrum of ground-state exciton transitions with subpicosecond time resolution. Our experimental concept is outlined in Fig. 15.2(a). We use spectrally broad femtosecond laser pulses which are centered around the excitonic QW absorption resonance and coupled into a near-field fiber probe to probe the optical QD nonlinearity. As a near-field probe we use an uncoated etched single mode optical fiber taper with a cone angle of about 30° [47]. With such probes we reach—in an illumination/collection geometry—a spatial resolution of about 150 nm, i.e., about $\lambda/5$ [41]. This high spatial resolution together with their large collection efficiency makes such uncoated fiber probes particularly well suited for semiconductor nanospectroscopy. Experimentally, we find that for GaAs samples about 1% of the light coupled into the fiber is collected in this illumination/collection geometry.

In the pump-probe experiments, the probe laser light reflected from the QW sample is collected by the same fiber probe, dispersed in an 0.5 m monochromator and then detected with a high-sensitivity liquid-nitrogen cooled CCD camera. This steady-state reflectivity spectrum $R_0(\omega_{\mathrm{det}})$ contains weak, spectrally narrow resonances from single QD transitions (Fig. 15.2(a)).

The interaction with a second pump pulse now affects the QD spectrum and thus gives rise to a modified probe reflectivity $R(\omega_{\mathrm{det}})$. Differential probe reflectivity spectra $\Delta R(\omega_{\mathrm{det}}, \Delta t)/R_0 = [R(\omega_{\mathrm{det}}, \Delta t) - R_0(\omega_{\mathrm{det}})]/R_0(\omega_{\mathrm{det}})$ are recorded at a fixed spatial position of the near-field tip as a function of the time delay Δt between pump and probe pulses. To probe the nonlinear optical response from single QDs, the high spatial resolution of the near-field technique is needed for two reasons. First, the

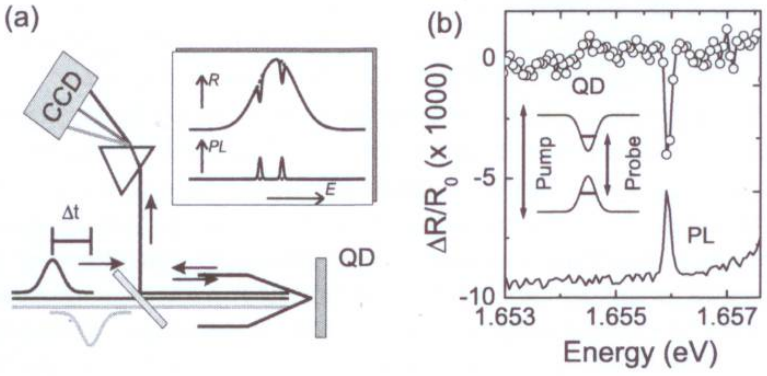

Fig. 15.2. (**a**) Schematic illustration of the experimental setup and of near-field PL and reflectivity spectra of a QD sample. (**b**) Near-field PL spectrum of a single QD (*solid line*) and differential reflectivity spectrum $\Delta R/R_0$ at $\Delta t = 30$ ps. PL and ΔR are recorded with identical pump pulses centered at 1.675 eV, exciting electron–hole pairs in 2D continuum states. The 100 nW probe pulses of 19 meV bandwidth are centered at 1.655 eV, around the QD absorption resonance. Inset: Schematic energy diagram

combined spatial and spectral resolution allows us to isolate single QD resonances (Fig. 15.1). Second, the relative amplitude of the QD resonance in $R_0(\omega_{\mathrm{det}})$ scales, in first approximation, inversely proportional to the square of the spatial resolution.

We assume for simplicity that the QD absorption spectrum can be modeled as that of an ideal two-level system (TLS) and that the incident laser power is homogeneously distributed over an area A (the areal resolution of the microscope). Then the incident power is $P = I_0 A$ and the absorbed power is $P_{\mathrm{QD}} = I_0 \sigma_{\mathrm{QD}}$, with I_0 being the incident intensity and σ_{QD} the QD absorption cross section. For an ideal TLS

$$\sigma_{\mathrm{QD}}(\omega) = \frac{\omega \mu_{\mathrm{QD}}^2}{nc\epsilon_0 \hbar} \frac{\gamma}{\gamma^2 + (\omega - \omega_{\mathrm{QD}}^2)}, \tag{15.1}$$

where $\omega_{\mathrm{QD}} = 2\pi c/\lambda_{\mathrm{QD}}$ denotes QD resonance frequency, ω the laser frequency, μ_{QD} the QD dipole moment, n the refractive index and $\gamma = 1/T_2$ the dephasing rate of the QD polarization. Improving the resolution from 1 μm to 100 nm increases the weak nonlinear QD signal by two orders of magnitude. For values typical for our experiments, $A = (250\,\mathrm{nm})^2$, $\mu_{\mathrm{QD}} = 60\,\mathrm{D}$, $\gamma = (30\,\mathrm{ps}^{-1})$, $n = 3.5$, $\lambda_{\mathrm{QD}} = 750\,\mathrm{nm}$, we estimate $\sigma_{\mathrm{QD}}/A \simeq 0.04$, certainly measurable with the sensitivity of our setup.

The near-field PL and differential reflectivity ΔR spectrum of a single QD are compared in Fig. 15.2(b). To record the ΔR spectrum we use 100-fs pump pulses derived from a 80 MHz repetition rate Ti:sapphire laser. The pump pulses in this experiment create less than five electron–hole pairs in QW states, corresponding to an excitation density of $5 \cdot 10^9\,\mathrm{cm}^{-2}$. Relaxation of these extra carriers into the QD bleaches the QD absorption and this bleaching is probed with 1 fJ probe pulses centered around the QW absorption resonance. Figure 15.2(b) depicts a differential reflectivity spectrum $\Delta R(E_{\mathrm{det}})$ at a time delay of 30 ps in the low-energy region of the 5.1 nm QW absorption spectrum. It displays a single spectrally sharp resonance at exactly the same spectral position E_{QD} as the simultaneously recorded near-field PL spectrum. The large amplitude of the signal of $5 \cdot 10^{-3}$ is consistent with a spatial resolution of the experiment of 200–250 nm. Two-dimensional spatial scans indicate a resolution of 230 nm, partly limited by the QD-to-surface distance.

To better understand the image contrast in these pump-probe experiments, we compare in Fig. 15.3 differential reflectivity $\Delta R(E_{\mathrm{det}})$ and PL spectra recorded under similar excitation conditions for single localized excitons in five different QWs buried at distances of 95–211 nm below the surface. We very clearly observe a transition between a dispersion-like and an absorption-like line shape as the QW-to-surface distance is varied. This behavior of the QD line shape can be understood in the framework of a local oscillator model as caused by the interference between the electric probe laser field $E_{\mathrm{R}}(t)$ reflected from the sample surface and the field $E_{\mathrm{QD}}(t)$ emitted from the QD in back direction. Our experiment works in the following way (Fig. 15.4). A fraction $E_{\mathrm{R}}(t)$ of the probe laser transmitted through the near-field probe is reflected from the sample surface and coupled back into the near field fiber probe. The probe field $E_{\mathrm{T}}(t)$, transmitted into the semiconductor, induces a polarization $P_{\mathrm{QD}}(t) = \int \mathrm{d}t' \chi_{\mathrm{QD}}(t') E_{\mathrm{T}}(t - t')$ of the QD located at a distance d below the sample surface. Here, $E_{\mathrm{T}}(t)$ and χ_{QD} denote the probe field interacting with the

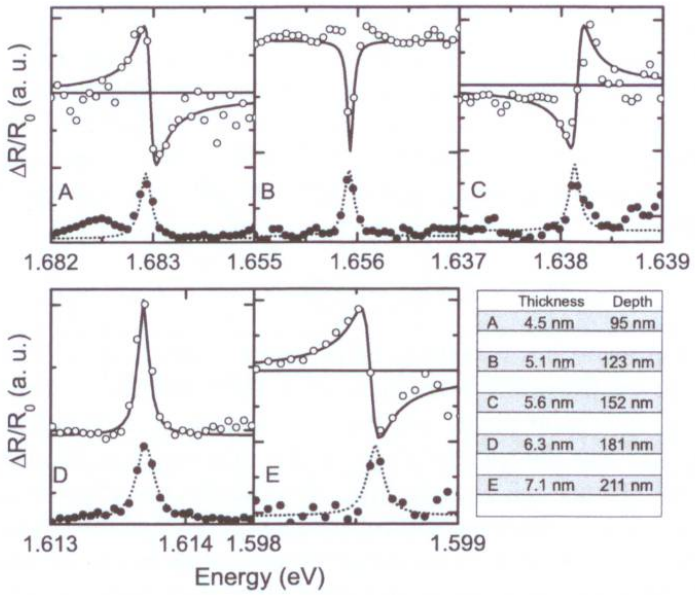

Fig. 15.3. Differential reflectivity spectra (*open circles*) of five interface QD located at different depths of 95–210 nm below the sample surface (see inset). The differential reflectivity spectra are compared to simultaneously recorded PL spectra. Note the transition between dispersive and absorptive line shapes

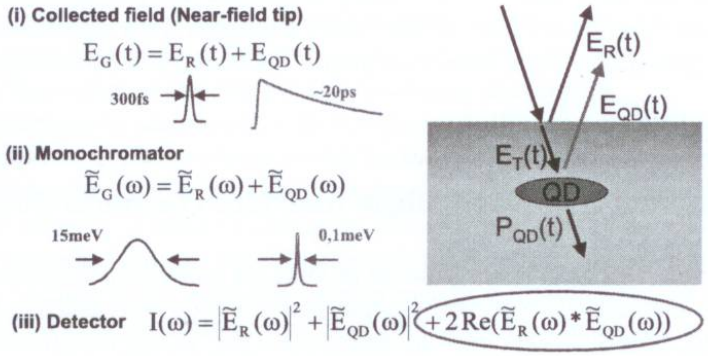

Fig. 15.4. Heterodyne detection of coherent QD polarizations. A femtosecond probe laser is coupled through a near-field fiber probe. A large fraction E_R of the probe laser is directly reflected the sample surface into the fiber probe. The transmitted probe light E_T is induces a QD dot polarization P_{QD} and the fraction E_{QD} of the electric field re-emitted from the QD is collected by the near-field probe. E_R and E_{QD} are spectrally dispersed in a monochromator and interfere on the CCD detector. This heterodyne detection scheme greatly enhances the weak QD field

QD and the QD susceptibility, respectively. The QD polarization re-emits an electric field and a fraction of this field, $E_{QD}(t)$ is locally collected by the near-field probe where it interferes with $E_R(t)$.

The time-integrated reflectivity $R(\omega)$ detected behind the monochromator is proportional to $|\tilde{E}_{\mathrm{QD}}(\omega) + \tilde{E}_{\mathrm{R}}(\omega)|^2 \simeq |\tilde{E}_{\mathrm{R}}(\omega)|^2 + 2\mathrm{Re}[\tilde{E}^*_{\mathrm{R}}(\omega)\tilde{E}_{\mathrm{QD}}(\omega)]$, where $\tilde{E}(\omega)$ denotes the Fourier transform of the field $E(t)$. Here, the finite monochromator resolution and the weak contribution from $|\tilde{E}_{\mathrm{QD}}|^2$ has been neglected. Excitation by the pump laser affects the QD polarization and thus results in a change of the QD reflectivity. The differential reflectivity $\Delta R(\omega, \Delta t)$ represents the spectral interferogram of $\tilde{E}_{\mathrm{R}}$ and $\tilde{E}_{\mathrm{QD}}$:

$$\Delta R(\omega, \Delta t) \propto \mathrm{Re}\{\tilde{E}^*_{\mathrm{R}}(\omega)[\tilde{E}_{\mathrm{QD}}(\omega, \Delta t) - \tilde{E}_{\mathrm{QD},0}(\omega)]\}. \tag{15.2}$$

The spectral shape of this interferogram evidently depends on the QD polarization dynamics and on the phase delay between $E_{\mathrm{QD}}(t)$ and $E_{\mathrm{R}}(t)$. Treating the QD for simplicity as a point dipole and the near-field tip as a point-like emitter, the phase delay and thus the spectral shape of this interferogram depends on the distance between QD and the near field tip. This interference effect is nicely seen in Fig. 15.3 and explains the transition between absorptive and dispersive line shapes. Since the QDs are buried below the surface by more than 50 nm, the near-field terms of the QD dipole emission can be neglected since they decay on a typical length scale of $\lambda/(2\pi n) \simeq 35$ nm ($n \simeq 3.5$—refractive index). Based on an optical path of $4\pi nd/\lambda$, we estimate a phase change of $\pi/2$ for a change in QD-sample distance of 28 nm. This is in quite good agreement with the results of Fig. 15.3. We consider this convincing evidence for the validity of the phenomenological local oscillator model described earlier. Clearly a detailed analysis of these data using, e.g., a Green function solution of Maxwell's equations for a realistic experimental geometry, is desirable for a more quantitative comparison between experiment and theory.

15.4 Coherent Control in Single Interface Quantum Dots

In this section, we describe experiments probing the coherent polarization dynamics of a single interface QD induced by impulsive excitation with ultrafast light pulses. Specifically, three different topics are addressed. First, we ask the fundamental questions: To what extent does the ultrafast nonlinear optical response of a single QD resemble that of an atomic system and how do many-body Coulomb interactions—often governing optical nonlinearities of higher-dimensional systems such as quantum wells and wires—affect the QD polarization dynamics? Then we demonstrate coherent control of the phase of the QD polarization by probing the optical Stark effect in a single QD and coherent control of the polarization amplitude by probing Rabi oscillations in single QD.

15.4.1 Ultrafast Optical Nonlinearities of Single Interface Quantum Dots

To study the effects of many-body interactions on the QD nonlinearities, we perform a quasi-two-color pump-probe experiment, exciting the QD sample in the QW

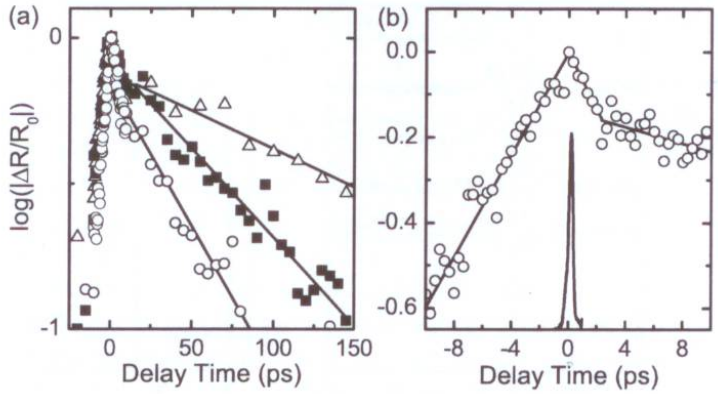

Fig. 15.5. (**a**) Temporal dynamics of $\Delta R/R_0$ for three different QD resonances (logarithmic ordinate scale). All decays are biexponential with a slow decay time varying between 30 and 150 ps. (**b**) Early time $\Delta R/R_0$ dynamics of a single QD resonance. A slow rise of $\Delta R/R_0$ is observed at negative time delays. The time resolution of the experiment is 150 fs, as indicated by the cross-correlation measurement (solid line around $\Delta t = 0$)

absorption continuum with 100 fs pump-pulses with a pulse energy of 1.5 fJ. These pulses create carriers in QW states and the resulting change in the QD spectrum is probed. The dynamics of the spectrally resolved reflectivity change measured on different QD resonances is shown in Fig. 15.5. After a picosecond rise of the signal at negative delay times (probe precedes pump) one finds a partial decay with a time constant of about 6 ps, followed by a much slower decay with time constants of 50–150 ps, depending on the specific QD resonance investigated.

The nonlinearities observed at sufficiently long positive Δt are easily understood on the basis of a simple two-level model for the QD nonlinearity. The pump pulse creates a nonequilibrium distribution of electron–hole pairs in QW continuum states. Subsequent trapping of these carriers gives rise to a bleaching of the QD absorption and a concomitant change of the QD reflectivity ΔR. Hence, the decay time of ΔR reflects the lifetime of the individual exciton state probed. Following an earlier conjecture [18], the QD population decay is mainly dominated by radiative recombination, i.e. $\tau_{\mathrm{rad}} \simeq \tau_{\mathrm{QD}}$. We can then estimate the dipole moment μ_{QD} of the individual QD using [46, 48]:

$$\frac{1}{\tau_{\mathrm{rad}}} = n\frac{\omega^3 \cdot \mu_{\mathrm{QD}}^2}{3\pi\epsilon_0\hbar c^3}. \tag{15.3}$$

We estimate dipole moments μ_{QD} of 50–85 Debye for τ_{rad} between 150 and 50 ps. These values are in rather good agreement with previous estimates [29, 48]. They exceed those of atomic systems by more than an order of magnitude and reflect the large spatial extension of the exciton center-of-mass wave function in these QDs. Near-field autocorrelation spectra indicate an exciton localization length of about 40–50 nm [49]. Due to the statistical nature of the disorder potential, the exciton localization length and thus the dipole moment and radiative recombination rate varies

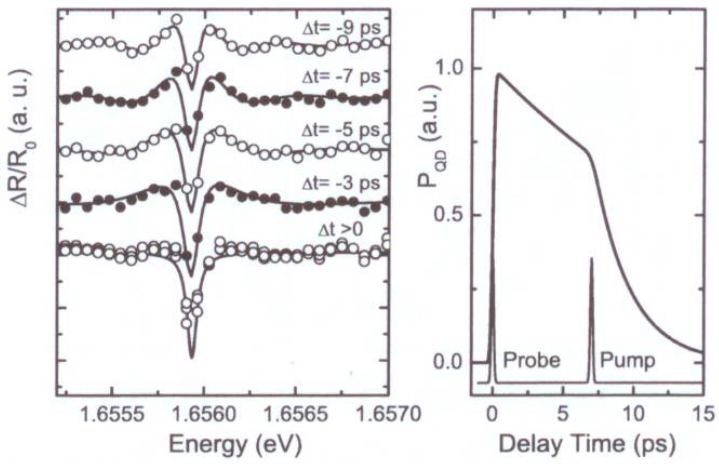

Fig. 15.6. (**a**) Near-field $\Delta R/R_0$ spectra (*circles*) at different delay times Δt. The spectra at $\Delta t < 0$ display pronounced spectral oscillations around the excitonic resonance. The solid lines show simulated spectra for the perturbed free induction decay of the coherent QD polarization assuming $T_2 = 15$ ps. (**b**) Dynamics of $P_{\mathrm{QD}}(t)$ extracted from the time dependent near-field $\Delta R/R_0$ spectra

quite strongly from QD to QD, as seen in Fig. 15.5(a). Theoretical models of localized excitons in disordered quantum wells [49, 50] yield comparable results.

The dynamics of the QD reflectivity on a time scale of less than 10 ps, however, are quite different from what is expected for an ideal atomic system. The time evolution shows an 8-ps rise at negative delay times, much slower than the 150-fs cross-correlation of pump and probe pulses. A biexponential decay is found at positive delays, where the slow component reflects the exciton lifetime as discussed earlier. The fast decay time of about 6 ps is similar for all different QDs. The spectral characteristics of the differential reflectivity are markedly different at positive and negative delays. At negative delays, pronounced spectrally symmetric oscillations around the excitonic resonance are observed (see Fig. 15.6). Their oscillation period decreases with increasing negative time delay. At large positive delays, the spectra show a bleaching of the QD resonance [34].

This complex behavior reflects directly the coherent polarization dynamics of the excitonic QD excitation. To account for this behavior, one has to consistently describe the dynamics of the field $E_{\mathrm{QD}}(t)$ radiated from the coherent QD polarization $P_{\mathrm{QD}}(t)$. We phenomenologically describe the QD as an effective two-level system with a ground (no-exciton) state $|0\rangle$, and an excited one-exciton state $|1\rangle$. Then the quantum state of the two-level system is given as a coherent superposition $|\psi(t)\rangle = c_0(t)|0\rangle + c_1(t)|1\rangle$. Within the density matrix formalism, $P_{\mathrm{QD}}(t)$ is given as $P_{\mathrm{QD}}(t) = \mu^*_{\mathrm{QD}}\rho_{01} + \mathrm{c.c.}$, where the microscopic QD polarization $\rho_{01} = \langle c^*_0 c_1\rangle$, μ_{QD} denotes the QD dipole moment and $\langle \ldots \rangle$ the ensemble average [51]. Then, the well-known Bloch equations hold and ρ_{01} obeys the equation of motion

$$\frac{\partial}{\partial t}\rho_{01}(t) = -\mathrm{i}\omega_{\mathrm{QD}}\rho_{01}(t) + \mathrm{i}(1 - 2n_{\mathrm{QD}})\omega_{\mathrm{R}} - \gamma\rho_{01}(t), \qquad (15.4)$$

with exciton energy ω_{QD}, dephasing rate γ, exciton population n_{QD} and generalized Rabi frequency ω_R.

In the absence of a pump laser, the resonant probe laser impulsively excites a coherent QD polarization which then decays with the dephasing rate γ (free induction decay). The re-emitted field interferes with the reflected probe laser field, giving rise to a Lorentzian QD line shape in $R_0(\omega)$. The fact that we observe a line width that is limited by our monochromator resolution of about 60 μeV gives a lower limit for the QD dephasing time of $T_2 = 1/\gamma > 15$ ps.

The transient spectral oscillations around the QD exciton resonance at negative time delays indicate that this free induction decay of $P_{QD}(t)$ is perturbed by the presence of the pump laser. In semiconductors, such oscillations have so far only been observed for higher dimensional system, e.g., studies of transient QW nonlinearities [52, 53]. In our experiments, the off-resonant pump does not directly interact with the QD dipole but creates electron–hole pairs (density n_{QW}) in the QW continuum. Many-body interactions between such carriers and the exciton that are mediated via the Coulomb interaction perturb the free induction decay of $P_{QD}(t)$.

The spectra at $\Delta t < 0$ are quantitatively described by assuming that an excitation-induced dephasing [54], i.e., an increase in γ due to the interaction between ρ_{01} and n_{QW} is the leading contribution to the QD nonlinearity at early times. Coulomb scattering between the QD dipole and the initial nonequilibrium carrier distribution in the QW causes this additional fast damping of ρ_{01}. In the frequency domain, this excitation-induced dephasing leads to oscillatory structures in the spectrum with a period determined by the time delay between probe and pump. The solid lines in Fig. 15.6(a) are calculated from (15.4) by assuming that the probe-induced QD polarization $P_{QD}(t)$ decays initially with an effective dephasing time $T_2 = 15$ ps, decreasing to $T_{EID} = 3$ ps after the arrival of the pump laser (Fig. 15.6(b)). Such an excitation-induced dephasing model accounts quantitatively for the transient oscillations and this analysis allows us to extract the QD polarization dynamics. A detailed theoretical analysis of the data was performed on the basis of the semiconductor Bloch equations in the mean-field approximation [34] and gives strong support for this interpretation.

Beyond the density-dependent dephasing processes leading to the perturbed free-induction decay, excitation of electrons and holes into continuum states gives rise to pump-probe signals at positive delay times, in particular the fast decay of the differential reflectivity at early delay times (Fig. 15.5(b)). Carriers initially populating continuum states relax into localized QD states, i.e., the population n_{QW} of QW states decays on a time scale of about 3 ps. Thus, the initial fast differential reflectivity decay reflects the transition from a QD nonlinearity dominated by excitation-induced dephasing to a nonlinearity dominated by exciton bleaching due to the population relaxation into the QDs.

These results highlight two important features of interface quantum dots. First, the coherence of the excitonic QD polarization persists for more than 10 ps even after resonant excitation with spectrally broadband femtosecond pulses. This decoherence time is two orders of magnitude larger than the duration of the excitation pulses. On the other hand, Coulomb many-body interactions may contribute signifi-

cantly to their optical nonlinearities on ultrashort time scales if an additional exciton population in quantum well continuum states is created during the optical excitation process. Such many-body interactions have to be taken into account as important additional dephasing mechanisms.

15.4.2 Rabi Oscillations in a Quantum Dot

In this section, we demonstrate coherent control of both the amplitude and phase of the coherent QD polarization on an ultrafast time scale. Coherent control of the population of a generic two-level system with finite electronic dipole moment $\boldsymbol{\mu}$ can be achieved by resonant impulsive excitation with light pulses much shorter in duration than the decoherence time of the microscopic polarization ρ_{01}. Neglecting for simplicity the finite decoherence time, the excited state population after the interaction with the excitation laser is given as $n_1 = \sin^2(\theta/2)$, with θ being the pulse area

$$\theta = \frac{\boldsymbol{\mu} \cdot \hat{\varepsilon}}{\hbar} \int_{-\infty}^{\infty} |E(t)| \, \mathrm{d}t, \tag{15.5}$$

where $E(t)$ denotes the time-dependent electric field of the excitation laser and $\hat{\varepsilon}$ its polarization direction. Thus, for weak excitation pulses the excited state population first increases linearly with increasing pulse intensity until it reaches a value of $n = 1$ for $\theta = \pi$, i.e., until the two-level system is fully inverted. Further increase in the pulse intensity induces stimulated emission from the excited state back to ground state and thus a decrease of excited state population. After interaction with a light pulse of area $\theta = 2\pi$ the excited state population reaches again $n = 0$, i.e. the system is back in its original state. For higher excitation, the population shows the well-known Rabi oscillations. This simplified picture only holds for resonant excitation and negligible decoherence, of course. Thus, the study of QD Rabi oscillations should generally give insight into the decoherence of quantum systems in the strong excitation regime.

For resonant excitation of only a single excitonic transition, we use spectrally tailored optical pulses with a spectral width of about 1 meV and a pulse duration of about 1.5 ps. We tune these pump pulses to a specific quantum dot resonance and probe the induced optical nonlinearity with collinearly polarized pulses of 15-meV spectral width and 200 fs duration. The idea of the experiment is to read out the transient exciton population by probing the induced absorption on the exciton–biexciton transition. Since each confined electron state in the QD can be occupied with two electrons of opposite spin orientation, two distinguishable single exciton states with orthogonal polarization can be optically excited. Simultaneous excitation of both exciton states results in a transient population of the bound biexciton state [Fig. 15.7(a)]. In interface QDs, the biexciton energy is normally slightly smaller (1–4 meV) than the sum of the two exciton energies due to the Coulombic interaction between the two excitons. Since the monolayer islands in interface quantum dots are slightly elongated along the [−110] direction [18], the energetic degeneracy of the two single-exciton states is lifted (by typically less than 100 μeV) [18]

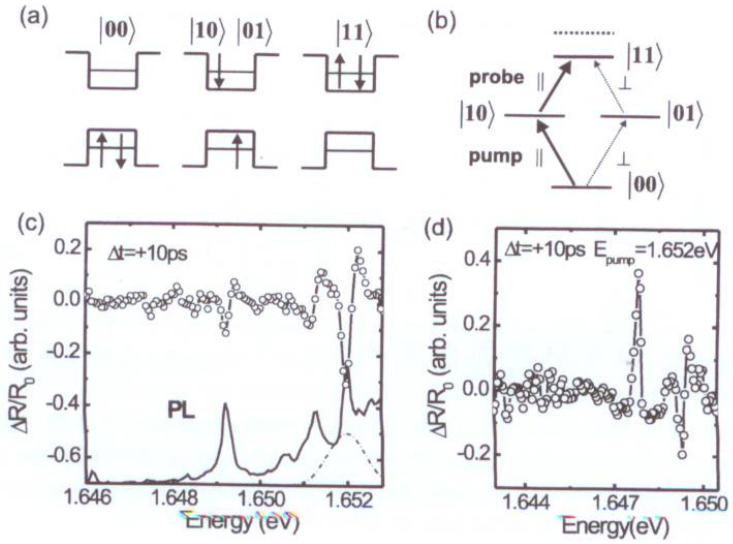

Fig. 15.7. (**a**) Schematics of exciton ground ($|00\rangle$), one-exciton ($|10\rangle$, and $|01\rangle$), and biexciton states $|11\rangle$ in a QD. (**b**) Excitation-level diagram in an interface QD and optical selection rules for pump and probe laser. (**c**) PL and ΔR for above-band gap excitation. In the studies of biexciton nonlinearities, the pump laser (*dashed line*) is tuned to the exciton resonance at 1.652 eV. (**d**) Pump-induced biexciton nonlinearity. The time delay between pump (at 1.652 eV) and probe laser is $\Delta t = 10$ ps

and one finds linear polarization selection rules for the exciton and biexciton transitions [18, 55]. The energy level structure of the QD states and the polarization selection rules can be summarized in a four-level system for the (no-exciton) crystal ground state $|00\rangle$, two exciton states with orthogonal polarization $|10\rangle$ and $|01\rangle$ and the biexciton state $|11\rangle$ [Fig. 15.7(b)]. Optical excitation of the $|00\rangle \rightarrow |10\rangle$ single exciton transition gives rise to excited state absorption on the $|10\rangle \rightarrow |11\rangle$ transition. This excited state absorption is not present in the absence of single exciton excitation.

In the experiment we observe, after single exciton excitation at 1.652 eV [Fig. 15.7(c)], a new transition at 1.648 eV, red-shifted by 4 meV from the single exciton transition which is assigned to the exciton–biexciton $X \rightarrow XX$ transition [Fig. 15.7(d)]. The dynamics of the pump-probe signal on the $X \rightarrow XX$ transition is consistent with this assignment [Fig. 15.8(a)]: There is no biexciton nonlinearity at negative delay times (probe precedes pump), i.e., in the absence of $|10\rangle$ exciton excitation. Around time zero the $X \rightarrow XX$ signal rises within the time resolution of the experiment and then decays exponentially on a 40-ps time scale with the radiative single exciton lifetime, demonstrating that the amplitude of the induced $X \rightarrow XX$ reflectivity change is a direct measure of the transient $|10\rangle$ exciton population generated by the pump pulse. The effect of the pump power on this biexciton nonlinearity is shown in Fig. 15.8(b) where the pump-probe signal ΔR_{XX} for a delay time of $\Delta t = 10$ ps is plotted vs. the maximum field strength $E_{\mathrm{pu}} \propto \sqrt{P_{\mathrm{pu}}}$ of

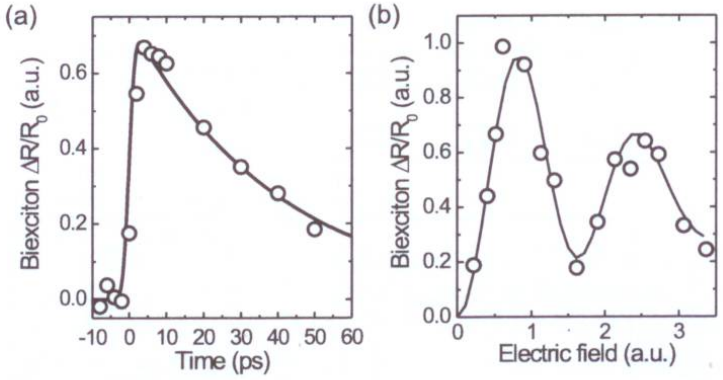

Fig. 15.8. (**a**) Temporal dynamics of the biexciton nonlinearity at 1.648 eV. The excitation conditions are as shown in Fig. 15.7. The 40-ps decay at $\Delta t > 0$ reflects the exciton lifetime. (**b**) Rabi oscillation in a single interface QD. Magnitude of the biexcition nonlinearity as function field amplitude of the pump laser at $\Delta t = 10$ ps

the pump pulse. The magnitude of the differential biexciton nonlinearity ΔR_{XX} displays pronounced oscillations, giving clear evidence for Rabi oscillations on a single ground-state exciton transition in a single interface QD. Despite the clarity of these oscillations, the experiment also shows that interface quantum dots are not an ideal two-level system. The biexcitonic nonlinearity at the second maximum, corresponding to a 3π excitation pulse, is about 1/3 smaller than that at the first maximum—corresponding to a π excitation. This unwanted damping of the Rabi oscillations is caused again by excitation-induced dephasing as an additional source of decoherence.

The field dependence of the biexciton nonlinearity, $\Delta R_{XX}(E_{\mathrm{pu}})$, is well reproduced within the framework of Optical Bloch Equations of a two-level system with an intensity-dependent dephasing rate $\gamma = 1/T_2 + \gamma_1 \cdot E_{\mathrm{pu}}^2$ [Fig. 15.8(b)]. Good agreement between experiment and model is achieved by assuming a dipole moment of 60 D, similar to those previously measured. The microscopic physics underlying this excitation-induced dephasing is similar to that reported for above-band gap excitation of QW continuum states in Sect. 15.4.1. Excitation by the picosecond pump pulse not only drives the desired single exciton transition but also creates coherent polarizations and incoherent populations in the QD environment. Since our pump-probe signals are accumulated over a large number of typically 10^8 laser pulses, these unwanted excitations give rise to fluctuating electric fields acting on the QD and, thus, to decoherence of the ensemble-averaged QD polarization. Our experimental results are well reproduced by assuming that the QD dephasing rate increases from less than $(15\,\mathrm{ps})^{-1}$ (an upper limit given by our finite monochromator resolution) to about $(6\,\mathrm{ps})^{-1}$ for a pulse area of 3π. In summary, these experiments show coherent control of the population of a single QD exciton through the demonstration of Rabi oscillations.

15.4.3 Optical Stark Effect: Ultrafast Control of Single Exciton Polarizations

Full coherent control over a single exciton excitation requires not only control over population—or more precisely the amplitude of the microscopic polarization ρ_{01}—but also control over the polarization phase $\phi = \arctan(\mathrm{Im}(\rho_{01})/\mathrm{Re}(\rho_{01}))$. In a Bloch sphere representation, which is often used to visualize the quantum dynamics of quasi-two-level systems, the momentary polarization ρ_{01} is represented as a three-dimensional vector $\rho_B = [\mathrm{Re}(\rho_{01}), \mathrm{Im}(\rho_{01})), 1/2(n_1 - n_0)]$, with $n_i = \langle c_i^* c_i \rangle$ describing the population of state $|i\rangle$. In this representation, polarization control thus means controlling the azimuthal angle ϕ in the $[\mathrm{Re}(\rho_{01}), \mathrm{Im}(\rho_{01})]$-plane.

Here we demonstrate control of the relative phase between the driving laser and the excitonic polarization by making use of the optical Stark effect (OSE). The OSE is one of the fundamental coherent light-matter interactions describing the light-induced shift ("dressing") of energy levels in the presence of nonresonant laser fields. In atomic systems the OSE is well known and, for weak excitation, well described by optical Bloch equations for independent two-level systems [56, 57]. In higher-dimensional semiconductors, e.g., quantum wells, however, the polarization dynamics induced by nonresonant light fields is much more complex than in atomic systems and often dominated by Coulomb-mediated many-body interactions [58–61]. Effects such as exciton–exciton interaction, biexciton formation or higher-order Coulomb correlations may affect the magnitude of the energy shift, the exciton oscillator strength and may even reverse the sign of the shift [60, 62–65]. Here, we report the first experimental study of the OSE in a single quasi-zero-dimensional semiconductor quantum dot [40].

Figure 15.9 compares the PL (solid line) from a single QD and the $\Delta R(\omega, \Delta t = 30\,\mathrm{ps})/R_0$ spectrum for above-band gap excitation of QW continuum states (solid circles). The absorptive ΔR spectrum reflects the bleaching of the QD resonance as described earlier. For below-band gap excitation, however, we observe for weak excitation ($P_{\mathrm{pu}} < 0.2\,\mu\mathrm{W}$) and negative delay times, $\Delta t = -4\,\mathrm{ps}$ (probe precedes pump), a dispersive line shape centered around ω_{QD}. With increasing excitation power, we find a drastic change in the line shape of $\Delta R(\omega)$ [Fig. 15.10(a)]: The signal maximum shifts slightly toward higher energies and an increasing number of spectral oscillations is observed, in particular on the high-energy side of the QD resonance. This change in line shape occurs together with a saturation of the strength of the nonlinear signal ΔR_{m}, taken as the difference between minimum and maximum of $\Delta R(\omega)$ [Fig. 15.10(b)]. As we will show in the following, this characteristic change in line shape allows us to extract the phase shift $\Delta\phi$ of the QD polarization due to the interaction with the off-resonant pump laser from a Bloch equation simulation. The extracted phase shift $\Delta\phi$ is plotted as a function of excitation power in Fig. 15.10(c).

To ensure that we are indeed probing only a light-induced shift of the exciton resonance, we also plot the time evolution of the QD nonlinearity $\Delta R_{\mathrm{m}}(\Delta t)/R_0$ (Fig. 15.11). It is important that the signal vanishes completely for positive delay times $\Delta t > 0$ (pump precedes probe) and rises around $\Delta t = 0$ within the time resolution of our experiment of 250 fs. For $\Delta t < 0$, $\Delta R(\Delta t)$ decays with a time constant of $\tau_{\mathrm{d}} = 8\,\mathrm{ps}$.

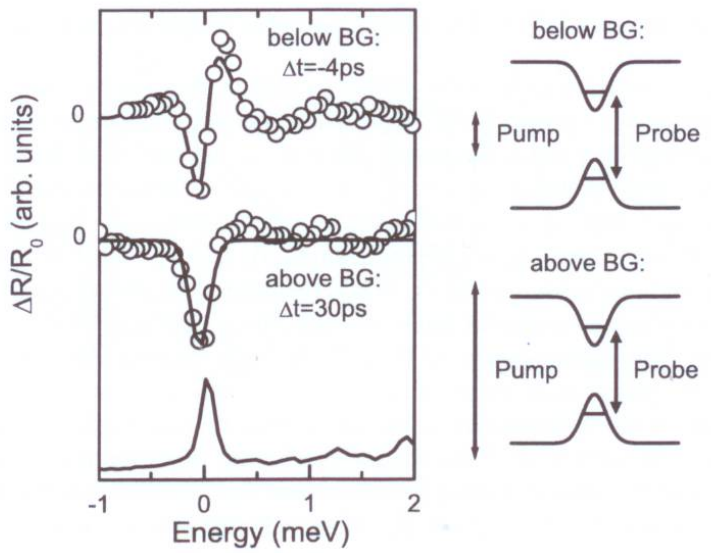

Fig. 15.9. (Left) PL spectrum of a single QD resonance $\omega_{QD} = 1.6503\,\text{eV}$ and differential reflectivity $\Delta R(\omega)/R_0$ for above-band gap excitation at $\Delta t = 30\,\text{ps}$ and for below-band gap excitation at $\Delta t = -4\,\text{ps}$ with 2-ps pulses at 1.647 eV (bandwidth $\sigma = 0.8\,\text{meV}$) in the weak excitation limit ($P_{pu} = 0.12\,\mu\text{W}$). Solid lines: Bloch equation model. (Right) Schematic excitation diagram

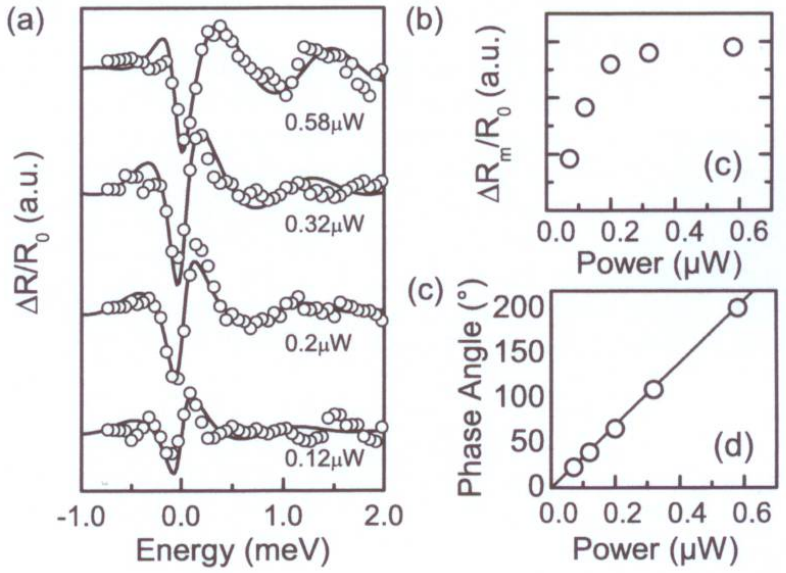

Fig. 15.10. (**a**) Optical Stark Effect in a single QD. Differential reflectivity spectra $\Delta R(\omega)/R_0$ for below-band gap excitation at $\Delta t = -4\,\text{ps}$ with 2-ps pulses at 1.647 eV (bandwidth $\sigma = 0.8\,\text{meV}$) for excitation powers between 0.12 and 0.58 μW. Solid lines: Bloch equation model. (**b**) Variation of the signal magnitude $\Delta R(\omega_{QD})/R_0$ with pump power. (**c**) Phase shift of the QD polarization vs. pump power

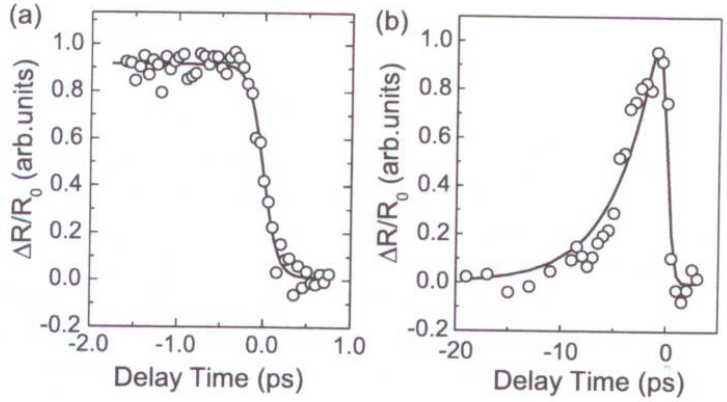

Fig. 15.11. Time evolution of $\Delta R(\Delta t)/R_0$ for a single QD at $\omega_{QD} = 1.6544$ eV. Here 200-fs pump pulses with a power of 58 μW were centered at 1.640 eV. $\Delta R_m(\Delta t > 0)$ vanishes and the signal for $\Delta t < 0$ decays on a ps time scale. (**a**) 3-ps time scale. (**b**) 25-ps time scale

The dispersive ΔR line shape observed in Fig. 15.9(a) for below-band gap excitation and small time delays is the signature of the OSE in the *weak excitation limit* [58]. It reflects a transient light-induced blue shift of the QD exciton resonance. In the presence of an AC electric field of frequency ω_p, the transition frequency of a two-level system shifts by $\Delta\omega_0(t) = \sqrt{[(\omega_0 - \omega_p)^2 + \Omega_R(t)^2]} + \omega_p - \omega_0$. Here, ω_0 is the transition frequency without external field, $\Omega_R(t) = \mu \cdot E_p(t)/\hbar$ is the Rabi frequency, μ the transition dipole moment and $E_p(t) \cdot \cos(\omega_p t)$ the (pump) AC electric field. The blue shift $\Delta\omega_0(t)$ of the QD absorption resonance results in a dispersive $\Delta R(\omega)/R_0$ line shape, which can be approximated as $\Delta R(\omega)/R_0 \propto \Delta\omega_{0,max} \cdot \partial\alpha(\omega)/\partial\omega$, where $\alpha(\omega)$ is the QD absorption spectrum and $\Delta\omega_{0,max}$ is the maximum blue shift. Thus, in the weak excitation limit, the amplitude of the $\Delta R(\omega)/R_0$ signal is expected to increase linearly with increasing pump power, without change of the line shape. The spectra of Fig. 15.10(a), taken with pump powers ≤ 0.2 μW, exactly display this behavior. For such pump powers, the Rabi frequency has a maximum value of $\Omega_{R,max} = 1.75$ meV $\simeq 5\Delta\omega_{0,max}$.

The origin of this transient blue shift becomes clear from an analysis of the optical Bloch equations. We describe the QD as a two-level system with a radiative lifetime of $T_1 = 100$ ps corresponding to a dipole moment $\mu = 50$ Debye [34, 45, 46]. A dephasing time of $T_2 = 8$ ps is assumed to account for our finite monochromator resolution. It is important to stress that since we know both power and duration τ_p of the pump pulses and the spatial resolution of about 250 nm, the electric field of the pump laser is estimated to within a factor of 2 and no free parameters enter the simulation.

The calculated dynamics of the QD polarization in the weak excitation limit are displayed in the rotating frame in Fig. 15.12(a). The probe field resonant to the exciton line changes the QD population and drives a coherent polarization oscillating at the QD resonance frequency ω_{QD}. This polarization is 90° phase-shifted with respect to the probe field ($\mathrm{Re}[P_{QD}] = 0$). During the presence of the pump

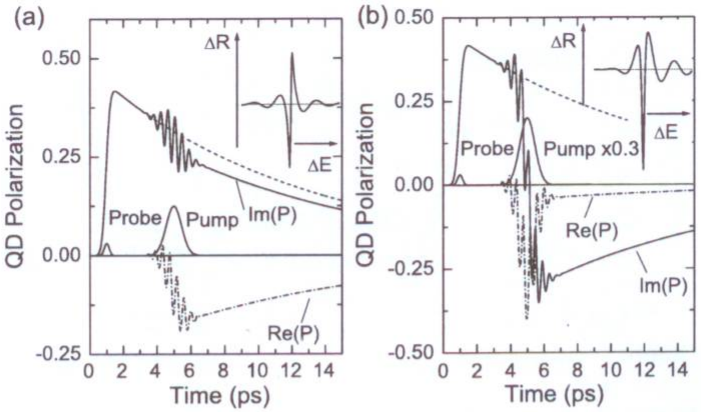

Fig. 15.12. Bloch equation simulation of the single QD optical Stark effect. Shown is the time-dependent QD polarization P_{QD} in the rotating frame with (*solid line*) and without (*dashed line*) pump laser. Nonlinear ΔR spectra are given in the inset. (**a**) Weak excitation limit. (**b**) Strong excitation limit. The chosen pump power corresponds to a phase shift $\Delta\phi = 172°$

pulse, the polarization is externally driven, leading to oscillations at the detuning frequency $\omega_{\mathrm{det}} = \omega_0 - \omega_{\mathrm{p}}$. After the interaction, the polarization is phase-shifted by $\Delta\phi \approx \int \Delta\omega_0(t)\,\mathrm{d}t$. It is this shift $\Delta\phi$ of the QD polarization which changes the product $E_{\mathrm{pr}}(\omega) \cdot E_{\mathrm{QD}}(\omega)$ of the complex electric fields and therefore the line shape. Fourier-transformation of the polarization dynamics gives directly the dispersive line shape of the $\Delta R(\omega)$ spectrum in the weak excitation limit, $\Delta\phi < 40°$, at early delay times (Fig. 15.9; inset in Fig. 15.12(a)).

The simulation also reproduces the time-dependent data shown in Fig. 15.11. Evidently, a vanishing nonlinearity at positive time delays is predicted by the Bloch model, since then the pump laser interacts with the sample before the excitonic polarization is created. At negative delays, the OSE nonlinearity is expected to decay with the dephasing time of the polarization. The fact that we reproduce both predictions of this simple model experimentally is quite striking. In particular we find, within our signal-to-noise ratio, no measurable nonlinearity at $\Delta t > 0$. This indicates that we are indeed probing a pure light-induced shift of the resonance and that nonlinearities induced by real carriers generated by one- or two-photon absorption in the surrounding of the QD obviously play a negligible role [40]. This conclusion is strongly supported by recording transient nonlinear spectra at different negative delay times between 0 and -10 ps. Here, pronounced spectral oscillations are observed which are quantitatively fit by the Bloch equation. Thus, even under femtosecond excitation, the nonlinear response of the interface QD for below-band gap excitation is very close to that of an isolated atomic system and it appears that the excitonic QD excitation is only weakly influenced by the complex solid state environment. To be precise, one should note that from our experiments one cannot directly tell whether the 8-ps decay at negative delay times reflects the polarization dephasing time. We are spectrally resolving the QD nonlinearity with a monochromator with

about 100 μeV resolution and this finite resolution puts an upper limit of slightly less than 10 ps to the measurable decay. Thus the 8-ps decay is close to our instrument resolution and gives a lower limit only for the excitonic decoherence rate.

For higher electric fields of the pump pulse, the weak excitation limit of the OSE nonlinearity is no longer valid. Experimentally, one finds additional features in the transient reflectivity spectra [Fig. 15.10(a), traces for pump intensities of 0.32 and 0.58 μW]. These spectral oscillations are a direct consequence of the interaction of the QD polarization with the strong pump field. The pump laser induces pronounced large amplitude oscillations of QD polarization at the detuning frequency during the presence of the pump laser. This is illustrated in Fig. 15.12(b) showing the solution of Bloch equations for strong excitation with $\Omega_R = 6\,\text{meV}$ ($\omega_{det} = -10\,\text{meV}$). A large phase shift $\Delta\phi$ of 172° of the QD polarization results from this interaction and the nonlinear ΔR spectrum shows additional oscillatory structures on the high-energy side, as found in the experiment. This large amplitude phase rotation corresponds to the observation of *gain* on the resonance of a single QD. In the Bloch sphere representation this phase rotation basically reflects a nutation-like motion of the Bloch vector, resulting in a change in azimuthal angle after the interaction. A comparison between experimental spectra and simulation [solid lines in Fig. 15.10(a)] allows us to quantify the phase shift $\Delta\phi$ experienced by the QD polarization. In Fig. 15.10(c) we plot $\Delta\phi$ obtained from the simulation of the data in Fig. 15.10(a) as a function of the pump power P_{pu}. We find a linear increase in $\Delta\phi$ with P_p. This means that the light shift also increases linearly in our experiment, despite the saturation of ΔR_m. This linear increase in the polarization phase $\Delta\phi$ is somewhat analogous to the pulse area theorem for Rabi oscillations of the population of a two-level system when driven with a resonant pulse. Currently, we can quantitatively measure the phase shift with an accuracy of about 10° and achieve phase rotations of as much as 200°. Control of the exciton density, on the other hand, has been established above by the observation of Rabi oscillations when varying the pulse area of a resonant excitation pulse. The result show that a sequence of a resonant and an off-resonant laser pulse gives full control over both amplitude *and* phase of the coherent excitonic polarization. In particular, we can switch the QD from absorption to gain within about 1 ps.

15.5 Coupling Two Quantum Dots via the Dipole–Dipole Interaction

Coherent control of excitonic transitions in a single QD, as demonstrated in the last section, is an essential prerequisite for exploring excitonic couplings between adjacent dots and attempting to implement potentially scalable two-qubit operations. Over the last few years, different microscopic coupling schemes have been proposed to theoretically achieve such implementations, among them couplings via photonic or plasmonic nanoresonator modes, via optical phonon wavepackets or through dipolar interactions. In particular, ultrafast optical realizations of two-qubit operations in dipole-coupled QDs have been studied theoretically in some detail [22, 23, 66–68].

So far, experimental studies of the proposed ideas have not been reported. This is partly due to a lack of suitable experimental methods. Since the strength of the dipole–dipole interaction depends strongly on both the geometric arrangment (orientation and separation of the dipoles) and on the microscopic interaction mechanism (permanent dipole couplings, van der Waals dispersion forces, Förster dipole energy transfer, etc.), studies of single nanosystems and/or ordered and homogeneous nanoarrays are often needed to resolve such couplings. Such experiments are scarce and have so far investigated a pair of molecules in an organic crystal [69] or the light-harvesting-2 complex [70] with steady-state techniques. Here, we demonstrate that combining high spatial resolution with time-resolving optical techniques allows us to separate different couplings through their individual real-time dynamics and control nanosystems on ultrashort time scales [39].

To probe dipole interactions between two individual QDs, we go back to the experimental situation depicted in Fig. 15.7. In Sect. 15.4.2 we discussed experiments demonstrating coherent population control of the QD resonance at an energy of 1.652 eV (QD A). In these experiments, we probed the pump-induced biexcitonic nonlinearity of this QD. The broad spectral bandwidth of the femtosecond probe pulses enables us to simultaneously probe the pump-induced nonlinear optical response of the other QDs detected at this NSOM tip position. We focus on the optical nonlinearity of the neighboring QD resonance at 1.649 eV (QD B) and study now the effect of a single-exciton excitation of QD A on the optical nonlinearity of this QD. Nonlinear spectra ΔR_{B} of QD B recorded with resonant excitation of QD A are displayed in Fig. 15.13(a). The excitation conditions are identical to those in Fig. 15.7(c) with an excitation pulse area of $\theta = 0.75\pi$.

Now, optical nonlinearities are observed at both positive *and* negative Δt, the latter being evident from the noninstantaneous rise of the signal in Fig. 15.13(b). In contrast to the absorptive line shape in Fig. 15.7(b), the nonlinear spectra display a time-independent dispersive line shape, reflecting a transient *blue* shift of the exciton resonance which does not change much with time delay. From the amplitude and shape of the nonlinear spectra we deduce a line shift of 30 ± 15 μeV around zero time delay. As seen in Fig. 15.13(b), the time evolution of $\Delta R_{\mathrm{B,m}}$, defined as the difference between maximum and minimum of $\Delta R_{\mathrm{B}}(\omega)$, is very different from that observed at the biexciton resonance. At negative time delays, $\Delta R_{\mathrm{B,m}}(\Delta t)$ shows a rise with a time constant of about 6 ps, followed by a slight dip and a slower decay on a time scale of more than 100 ps. The change of $\Delta R_{\mathrm{B,m}}$ with the excitation field displays clear Rabi oscillations.

To discuss these results, we stress the following observations: (i) Dispersive line shapes, caused by a transient blue shift of the QD resonance, are observed at all time delays and we find no signature of absorptive ΔR changes which would reflect pump-induced changes of the exciton population of QD B. This indicates that the observed nonlinearity is not due to an exciton relaxation between QD A and B. (ii) The presence of a strong laser field gives rise to transient excitonic line shifts via the optical Stark effect (OSE). However, as shown in Sect. 15.4.3, the OSE leads to optical nonlinearities at negative time delays ($\Delta t < 0$) only. Also, for a pump frequency above the exciton resonance, a red-shift of the QD line is expected, in contradiction

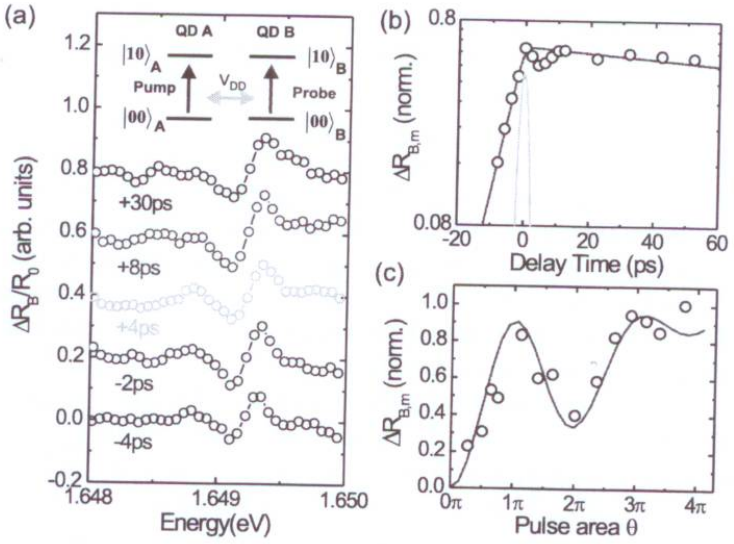

Fig. 15.13. (**a**) Nonlinear ΔR spectra of quantum dot B for resonant single-exciton excitation of QD A at 1.652 eV as a function of time delay Δt. The pulse area of the 2-ps excitation pulses is $\theta \simeq 0.75\pi$. Inset: Excitonic $|00\rangle \rightarrow |10\rangle$ transitions in QD A and QD B coupled through V_{DD}. (**b**) Time dynamics of $\Delta R_B(\Delta t)$. The excitation conditions are the same as in (**a**) and the time resolution of the experiment is indicated (*thin solid line*). (**c**) Rabi oscillation in a coupled QD. Magnitude of $\Delta R_B(\Delta t = 10\,\text{ps})$ as a function of the field amplitude of the pump laser. The solid line shows a simulation based on an optical Bloch equation model

with our present findings. (iii) There is a clear correlation between the pulse-area dependence of ΔR_{XX} in Fig. 15.8(b) and of ΔR_B in Fig. 15.13(c).

The data in Fig. 15.13 thus reflect an electronic coupling between the QDs A and B. The most likely candidate for such an interaction is a dipole–dipole coupling between both QDs. Theoretical studies [22, 23, 66, 67] indicate that two different mechanisms can contribute: resonant Förster energy transfer and direct Coulomb interaction between permanent excitonic dipole moments. For two quantum dots separated by less than the wavelength of light, pulsed optical excitation of one QD leads to the re-emission of a transient electric field which can be reabsorbed by the second QD, thus (Förster) transferring the excitation. The interaction Hamiltonian $H_F = V_F p_A p_B^* + \text{c.c.}$ includes the coupling $V_F \propto \mu_A \mu_B / R_{AB}^3$ between coherent excitonic polarizations $p_i(t) = |10\rangle_i\langle 01|_i + \text{c.c.}$ in QDs A and B. The coupling strength is determined by the transition dipole moments $\mu_i = |\langle 00|\boldsymbol{M}_i|10\rangle_i|$ ($\boldsymbol{M}_i$: dipole operator) and the QD separation R_{AB}. In the strong coupling limit, $V_F/\hbar$ is larger than the detuning $\Delta\omega = \omega_A - \omega_B$ between the QD resonances and the dephasing rate $1/T_2$, leading to entangled states of the coupled system and cooperative effects in its radiative decay [67, 69, 71]. In the weak coupling limit, $V_F \ll \hbar\Delta\omega, \hbar/T_2$, the interaction induces a population relaxation between the coupled states [72].

The direct dipole interaction H_D on the other hand involves permanent excitonic dipole moments and thus interaction between the exciton populations $n_i = |10\rangle_i\langle 10|_i$

with $H_D = V_D n_A n_B$ and $V_D \propto d_A d_B / R_{AB}^3$. Here, d_i represents the permanent dipole moment originating from a shift of the electron and hole charge distributions in the exciton. This interaction leads to a biexcitonic energy shift V_D in case that both QDs are excited [22].

To examine these two interaction mechanisms, nonlinear optical spectra are calculated from the time evolution of the density matrix in rotating wave approximation. Here, the QDs are treated as effective two-level systems (states $|00\rangle_i$, $|10\rangle_i$), interacting with the pump and probe fields and coupled via the dipole–dipole interaction. Most of the parameters of these calculations, such as ω_i, μ_i, $T_{2,i}$, and electric field profiles of the lasers are quantitatively known. The basic unknown is the mechanism and strength of the dipole–dipole interaction.

For the Förster mechanism, the time-evolution of the spectra depends critically on the ratios of V_F, $\hbar\Delta\omega$, and $\hbar/T_2$. In our case, typical interdot distances are limited by the finite exciton size to about 20 nm, giving $V_F \simeq 30\,\mu\text{eV}$ for $\mu = 60\,\text{D}$. Therefore $V_F \leq \hbar/T_2$ (0.1 meV) $\ll \hbar\Delta\omega$ (3 meV), i.e., we are in the weak coupling limit. At negative delay times $\Delta t < 0$, $\Delta R_{B,m}$ is due to the optical Stark effect induced by the pump field with a dispersive line shape reflecting a red shift of the exciton line, and a rise of $\Delta R_{B,m}(\Delta t < 0)$ with $T_{2,B}$ (Fig. 15.14(a)). At $\Delta t > 0$, the Förster mechanism induces exciton population relaxation between both QDs, resulting in absorptive line shapes. The decay of $\Delta R_{B,m}(\Delta t > 0)$ reflects both the exciton lifetime $T_{1,A} \simeq 40\,\text{ps}$ and the exciton transfer rate which scales as $\Gamma_F \propto V_F^2 T_2 [1 + (\Delta\omega T_2)^2]^{-1}$ [72]. Although the excitation field dependence of $\Delta R_{B,m}(\Delta t = 10\,\text{ps})$ (Fig. 15.14(c)) displays Rabi oscillations, the line shapes and the temporal dynamics of $\Delta R_{B,m}$ are in disagreement with the experiment. Also the amplitude of $\Delta R_{B,m}$ is much smaller than in the experiment. We infer that dipole coupling via the Förster mechanism is of minor importance for our QDs.

For a direct dipole interaction H_D between permanent excitonic dipole moments, excitation of QD A transiently shifts the energy of QD B by V_D. The sign of this shift depends on the sign of V_D and, thus, a blue shift occurs for parallel dipoles d_A and d_B. For a shift smaller than the homogeneous exciton line width, the coupling results in a dispersive shape of ΔR (Fig. 15.14(b)). Both direct dipole coupling and OSE contribute to the line shifts at $\Delta t < 0$ and net blue shifts are observed if the Coulomb coupling is stronger than the OSE. The signal at $\Delta t < 0$ rises with $T_{2,B}$. For $\Delta t > 0$, $\Delta R_{B,m}$ decays exponentially with the exciton lifetime $T_{1,A}$, as there is no population transfer between the dots. The amplitude of $\Delta R_{B,m}$ monitors the exciton population in QD A and the intensity dependence of the pump-induced Rabi oscillation (Fig. 15.14(b)) is thus similar to that found in the single exciton manipulation experiments.

The experimental line shapes and Rabi oscillations are in good agreement with the direct coupling model. The calculated decay of $\Delta R_{B,m}$, however, is faster. This discrepancy may reflect signal contributions from more delocalized excitonic transitions in the environment of QD A [42]. Such states have smaller dipole moments and thus longer radiative lifetimes. Their presence may also lead to finite dipole shifts that persist on time scales longer than $T_{1,A}$. This notion is supported by finding experimentally a finite optical nonlinearity from QD B when the excitation pulse is

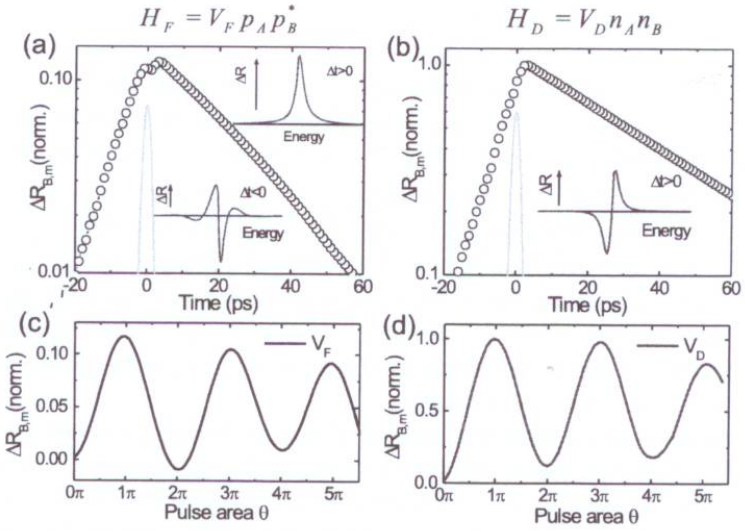

Fig. 15.14. (**a**) Simulation of optical nonlinearities of two QDs coupled by Förster energy transfer for excitation conditions similar to Fig. 15.13. The nonlinear spectra (inset) display an absorptive line shape at $\Delta t > 0$ and dispersive red-shifted line shape at $\Delta t < 0$. (**b**) Coupling via permanent excitonic dipole moments. For $V_D > 0$, the nonlinear spectra (inset) reflect a blue shift of the exciton line at all time delays. Pump-induced Rabi oscillations ($\Delta t = 10$ ps) for (c) Förster and (**d**) direct dipole coupling

slightly detuned from the resonance of QD A. For such a nonresonant excitation, however, Rabi oscillations are not observed. This indicates that the direct coupling between permanent excitonic dipole moments is the dominant interaction mechanism. Apart from the permanent dipoles, the Coulomb interaction between excitons in QD A and B may lead to induced charge rearrangements which lower the energy (formation of distant biexcitons). The absence of a redshift in the experiment points to a dominance of dipole repulsion over such correlation effects.

It is interesting to ask whether the weak Förster coupling is a general property of this class of QD samples. The energy statistics of the localized exciton states are heavily influenced by level repulsion effects [42], resulting in finite energy splittings between excitons in neighboring QDs. Such splittings are typically 1–3 meV and thus stronger than the dipole coupling. Thus, it is quite unlikely to find near-resonance situations between adjacent QDs and Förster coupling is expected to be weak in general.

15.6 Summary and Conclusions

We introduced a novel technique—ultrafast near-field optical spectroscopy—to probe the nonlinear optical response of single semiconductor quantum dots. We used this technique to demonstrate coherent control over amplitude and phase of the excitonic QD polarization. Rabi oscillations of up to 4π are induced and probed by ultrashort

light pulses. It appears that even in relatively weakly confined interface quantum dots, the ultrafast polarization dynamics are in many respects similar to those of an atomic system, yet with an enhanced dipole moment. Only when interacting with strong excitation pulses with an area of order 2π, excitation-induced dephasing due to Coulomb-mediated many-body interactions is limiting the visibility of Rabi oscillations. One may expect that using quantum dots with larger confinement energies may reduce excitation-induced dephasing. Yet so far the experiments on Rabi oscillations in more strongly confined self-assembled quantum dots seem to indicate that other factors, such as enhanced exciton–phonon coupling, may be important additional decoherence sources. Certainly, the microscopic origin of exciton decoherence in single quantum dots will be the topic of much additional experimental and theoretical work in the near future.

We introduced an experimental technique that probes transient optical nonlinearities in a broad spectral range and thus is particularly well suited to study excitonic couplings. This allowed us to demonstrate coupling between permanent excitonic dipole moments in a pair of adjacent quantum dots. The coupling strength of about 30 μeV is still about one order of magnitude too small to implement a nonlocal conditional quantum gate as proposed in [22]. An increase in coupling should readily be achievable by applying moderate lateral electric fields and two-qubit gating times of a few picoseconds seem feasible [23].

Recent progress in nanofabrication allows for manufacturing linear arrays of vertically and laterally stacked quantum dots with well-defined interdot distances. Such systems may permit us to go beyond two-qubit operations toward scalable qubit arrays, even though statistical variations of the coupling parameters within such arrays and excitation-induced decoherence still pose major technological challenges. Either energy-selective addressing (with inherently limited scalability) or cellular-automaton schemes with globally applied multicolor pulse sequences may be used for encoding information in such arrays. The now-established real-time probing of many-body interactions between individual solid-state nanostructures will certainly be of key importance for future progress in this area.

Acknowledgment

We thank Francesca Intonti, Tobias Guenther, Kerstin Mueller, and Thomas Unold for their important contributions to the work reviewed here. High-quality semiconductor samples were provided by Soheyla Eshlaghi and Andreas D. Wieck (Ruhr-Universität Bochum). We are very grateful for theoretical support from and stimulating discussion with Markus Glaneman, Vollrath Martin Axt and Tilmann Kuhn (Universität Münster), Andreas Knorr (Technische Universität Berlin), and Roland Zimmermann (Humboldt-Universität Berlin). Financial support by the Deutsche Forschungsgemeinschaft (SFB296) and the European Union through the SQID program is gratefully acknowledged.

References

1. M.A. Nielsen, I.L. Chuang, *Quantum Computation and Quantum Information* (Cambridge University Press, Cambridge, 2000)
2. N. Gershenfeld, I.L. Chuang, Bulk spin-resonance quantum computation. Science **275**, 350 (1997)
3. L.M.K. Vandersypen, M. Steffen, G. Breyta, C.S. Yannoni, M.H. Sherwood, I.L. Chuang, Experimental realization of Shor's quantum factoring algorithm using nuclear magnetic resonance. Nature **414**, 883 (2001)
4. J.C. Cirac, P. Zoller, Quantum computations with cold trapped ions. Phys. Rev. Lett. **74**, 4091 (1995)
5. A. Sorensen, K. Molmer, Quantum computation with ions in thermal motion. Phys. Rev. Lett. **82**, 1971 (1999)
6. S. Gulde, M. Riebe, G.P.T. Lancaster, C. Becher, J. Eschner, H. Häffner, F. Schmidt-Kaler, I.L. Chuang, R. Blatt, Implementation of the Deutsch-Jozsa algorithm on an ion-trap quantum computer. Nature **421**, 48 (2003)
7. F. Schmidt-Kaler, H. Häffner, M. Riebe, S. Gulde, G.P.T. Lancaster, T. Deuschle, C. Becher, C.F. Roos, J. Eschner, R. Blatt, Realization of the Cirac-Zoller controlled-NOT quantum gate. Nature **422**, 408 (2003)
8. Q.A. Turchette, C.J. Hood, W. Lange, H. Mabuchi, H.J. Kimble, Measurement of conditional phase shifts for quantum logic. Phys. Rev. Lett. **75**, 4710 (1995)
9. G.K. Brennen, C.M. Caves, I.H. Deutsch, Quantum logic gates in optical lattices. Phys. Rev. Lett. **82**, 1060 (1999)
10. M. Woldeyohannes, S. John, Coherent control of spontaneous emission near a photonic band edge: A qubit for quantum computation. Phys. Rev. A **60**, 5046 (1999)
11. J.E. Mooij, T.P. Orlando, L. Levitov, L. Tian, C.H. van der Wal, S. Lloyd, Josephson persistent-current qubit. Science **285**, 1036 (1999)
12. T. Yamamoto, Y.A. Pashkin, O. Astafiev, Y. Nakamura, J.S. Tsai, Demonstration of conditional gate operation using superconducting charge qubits. Nature **425**, 941 (2003)
13. J.D. Franson, Cooperative enhancement of optical quantum gates. Phys. Rev. Lett. **78**, 3852 (1997)
14. E. Knill, R. Laflamme, G.J. Milburn, A scheme for efficient quantum computation with linear optics. Nature **409**, 46 (2001)
15. A. Zrenner, A close look on single quantum dots. J. Chem. Phys. **112**, 7790 (2000)
16. K. Brunner, G. Abstreiter, G. Böhm, G. Tränkle, G. Weimann, Sharp-line photoluminescence and two-photon absorption of zero-dimensional biexcitons in a GaAs/AlGaAs structure. Phys. Rev. Lett. **73**, 1138 (1994)
17. H.F. Hess, E. Betzig, T.D. Harris, L.N. Pfeiffer, K.W. West, Near-field spectroscopy of the quantum constituents of a luminescent system. Science **264**, 1740 (1994)
18. D. Gammon, E.S. Snow, B.V. Shanabrook, D.S. Katzer, D. Park, Fine structure splitting in the optical spectra of single GaAs quantum dots. Phys. Rev. Lett. **76**, 3005 (1996)
19. P. Hawrylak, G.A. Narvaez, M. Bayer, A. Forchel, Excitonic absorption in a quantum dot. Phys. Rev. Lett. **85**, 389 (2000)
20. P. Borri, W. Langbein, S. Schneider, U. Woggon, R.L. Sellin, D. Ouyang, D. Bimberg, Ultralong dephasing time in InGaAs quantum dots. Phys. Rev. Lett. **87**, 157401 (2001)
21. M. Bayer, A. Forchel, Temperature dependence of the exciton homogeneous linewidth in In0.60Ga0.40As/GaAs self-assembled quantum dots. Phys. Rev. B **65**, 041308 (2002)
22. E. Biolatti, R. Iotti, P. Zanardi, F. Rossi, Quantum information processing with semiconductor macroatoms. Phys. Rev. Lett. **85**, 5647 (2000)

23. E. Biolatti, I. D'Amico, P. Zanardi, F. Rossi, Electro-optical properties of semiconductor quantum dots: Application to quantum information processing. Phys. Rev. B **65**, 075306 (2002)
24. P. Chen, C. Piermarocchi, L.J. Sham, Control of exciton dynamics in nanodots for quantum operations. Phys. Rev. Lett. **87**, 067401 (2001)
25. C. Piermarocchi, P. Chen, Y.S. Dale, L.J. Sham, Theory of fast quantum control of exciton dynamics in semiconductor quantum dots. Phys. Rev. B **65**, 075307 (2002)
26. N.H. Bonadeo, G. Chen, D. Gammon, D.S. Katzer, D. Park, D.G. Steel, Nonlinear nano-optics: probing one exciton at a time. Phys. Rev. Lett. **81**, 2759 (1998)
27. Y. Toda, T. Sugimoto, M. Nishioka, Y. Arakawa, Near-field coherent excitation spectroscopy of InGaAs/GaAs self-assembled quantum dots. Appl. Phys. Lett. **76**, 3887 (2000)
28. T. Flissikowski, A. Hundt, M. Lowisch, M. Rabe, F. Henneberger, Photon beats from a single semiconductor quantum dot. Phys. Rev. Lett. **86**, 3172 (2001)
29. T.H. Stievater, X. Li, D.G. Steel, D. Gammon, D.S. Katzer, D. Park, C. Piermarocchi, L.J. Sham, Rabi oscillations of excitons in single quantum dots. Phys. Rev. Lett. **87**, 133603 (2001)
30. H. Kamada, H. Gotoh, J. Temmyo, T. Takagahara, H. Ando, Exciton Rabi oscillation in a single quantum dot. Phys. Rev. Lett. **87**, 246401 (2001)
31. H. Htoon, T. Takagahara, D. Kulik, O. Baklenov, A.L. Holmes Jr., C.K. Shih, Interplay of Rabi oscillations and quantum interference in semiconductor quantum dots. Phys. Rev. Lett. **88**, 087401 (2002)
32. A. Zrenner, E. Beham, S. Stuffer, F. Findeis, M. Bichler, G. Abstreiter, Coherent properties of a two-level system based on a quantum-dot photodiode. Nature **418**, 612 (2002)
33. L. Besombes, J.J. Baumberg, J. Motohisa, Coherent spectroscopy of optically gated charged single InGaAs quantum dots. Phys. Rev. Lett. **90**, 257402 (2003)
34. T. Guenther, C. Lienau, T. Elsaesser, M. Glanemann, V.M. Axt, T. Kuhn, S. Eshlaghi, A.D. Wieck, Coherent nonlinear optical response of single quantum dots studied by ultrafast near-field spectroscopy. Phys. Rev. Lett. **89**, 057401 (2002), Erratum Phys. Rev. Lett. **89**, 179901 (2002)
35. A. Vagov, V.M. Axt, T. Kuhn, Electron-phonon dynamics in optically excited quantum dots: Exact solution for multiple ultrashort laser pulses. Phys. Rev. B **66**, 165312 (2002)
36. J. Förstner, C. Weber, J. Danckwerts, A. Knorr, Phonon-assisted damping of Rabi oscillations in semiconductor quantum dots. Phys. Rev. Lett. **91**, 127401 (2003)
37. X. Li, Y. Wu, D. Steel, D. Gammon, T.H. Stievater, D.S. Katzer, D. Park, C. Piermarocchi, L.J. Sham, An all-optical quantum gate in a semiconductor quantum dot. Science **301**, 809 (2003)
38. T. Guenther, C. Lienau, T. Elsaesser, M. Glanemann, V.M. Axt, T. Kuhn, Guenther et al. Reply. Phys. Rev. Lett. **90**, 139702 (2003)
39. T. Unold, K. Mueller, C. Lienau, T. Elsaesser, A.D. Wieck, Optical control of excitons in a pair of quantum dots coupled by the dipole–dipole interaction. Phys. Rev. Lett. **94**, 137404 (2005)
40. T. Unold, K. Mueller, C. Lienau, T. Elsaesser, A.D. Wieck, Optical Stark effect in a quantum dot: ultrafast control of single exciton polarizations. Phys. Rev. Lett. **92**, 157401 (2004)
41. F. Intonti, V. Emiliani, C. Lienau, T. Elsaesser, R. Nötzel, K.H. Ploog, Near-field optical spectroscopy of localized and delocalized excitons in a single GaAs quantum wire. Phys. Rev. B **63**, 075313 (2001)

42. F. Intonti, V. Emiliani, C. Lienau, T. Elsaesser, V. Savona, E. Runge, R. Zimmermann, R. Nötzel, K.H. Ploog, Quantum mechanical repulsion of exciton levels in a disordered quantum well. Phys. Rev. Lett. **87**, 076801 (2001)
43. V. Emiliani, F. Intonti, C. Lienau, T. Elsaesser, R. Nötzel, K.H. Ploog, Near-field optical imaging and spectroscopy of a coupled quantum wire-dot structure. Phys. Rev. B **64**, 155316 (2001)
44. D. Gammon, E.S. Snow, B.V. Shanabook, D.S. Katzer, D. Park, Homogeneous liniwidths in the optical spectrum of a single gallium arsenide quantum dot. Science **273**, 87 (1996)
45. J.R. Guest, T.H. Stievater, X. Li, J. Cheng, D.G. Steel, D. Gammon, D.S. Katzer, D. Park, C. Ell, A. Thränhardt, G. Khitrova, H.M. Gibbs, Measurement of optical absorption by a single quantum dot exciton. Phys. Rev. B **65**, 241310(R) (2002)
46. A. Thränhardt, C. Ell, G. Khitrova, H.M. Gibbs, Relation between dipole moment and radiative lifetime in interface quantum dots. Phys. Rev. B **65**, 035327 (2002)
47. P. Lambelet, A. Sayah, M. Pfeffer, C. Philipona, F. Marquis-Weible, Chemically etched fiber tips for near-field optical microscopy: A process for smoother tips. Appl. Opt. **37**, 7289 (1998)
48. L.C. Andreani, G. Panzarini, J.M. Gerard, Strong-coupling regime for quantum boxes in pillar microcavities: Theory. Phys. Rev. B **60**, 13276 (1999)
49. C. Lienau, F. Intonti, T. Guenther, T. Elsaesser, V. Savona, R. Zimmermann, E. Runge, Near-field autocorrelation spectroscopy of disordered semiconductor quantum wells. Phys. Rev. B **69**, 085302 (2004)
50. V. Savona, E. Runge, R. Zimmermann, F. Intonti, V. Emiliani, C. Lienau, T. Elsaesser, Level repulsion of localized excitons in disordered quantum wells. Phys. Stat. Sol. (a) **190**, 625 (2002)
51. H. Haug, S.W. Koch, *Quantum Theory of the Optical and Electronic Properties of Semiconductors*, 2nd edn. (World Scientific, Singapore, 1994)
52. B. Fluegel, N. Peyghambarian, G. Olbright, M. Lindberg, S.W. Koch, M. Joffre, D. Hulin, A. Migus, A. Antonetti, Femtosecond studies of coherent transients in semiconductors. Phys. Rev. Lett. **59**, 2588 (1987)
53. J.P. Sokoloff, M. Joffre, B. Fluegel, D. Hulin, M. Lindberg, S.W. Koch, A. Migus, A. Antonetti, N. Peyghambarian, Transient oscillations in the vicinity of excitons and in the band of semiconductors. Phys. Rev. B **38**, 7615 (1988)
54. H. Wang, K. Ferrio, D.G. Steel, Y.Z. Hu, R. Binder, S.W. Koch, Transient nonlinear optical response from excitation induced dephasing in GaAs. Phys. Rev. Lett. **71**, 1261 (1993)
55. A. Bertoni, P. Bordone, R. Brunetti, C. Jacoboni, S. Reggiani, Quantum logic gates based on coherent electron transport in quantum wires. Phys. Rev. Lett. **84**, 5912 (2000)
56. B.R. Mollow, Stimulated emission and absorption near resonance for driven systems. Phys. Rev. A **5**, 2217 (1972)
57. H. Häffner, S. Gulde, M. Riebe, G. Lancaster, C. Becher, J. Eschner, F. Schmidt-Kaler, R. Blatt, Precision measurement and compensation of optical Stark shifts for an ion-trap quantum processor. Phys. Rev. Lett. **90**, 143602 (2003)
58. A. Mysyrowicz, D. Hulin, A. Antonetti, A. Migus, W.T. Masselink, H. Morkoç, "Dressed excitons" in a multiple-quantum-well structure: Evidence for an optical Stark effect with femtosecond response time. Phys. Rev. Lett. **56**, 2478 (1986)
59. W.H. Knox, D.S. Chemla, D.A.B. Miller, J.B. Stark, S. Schmitt-Rink, Femtosecond ac Stark effect in semiconductor quantum wells: Extreme low- and high-intensity limits. Phys. Rev. Lett. **62**, 1189–1192 (1989)
60. C. Sieh, T. Meier, F. Jahnke, A. Knorr, S.W. Koch, P. Brick, M. Hübner, C. Ell, J. Prineas, G. Khitrova, H.M. Gibbs, Coulomb memory signatures in the excitonic optical Stark effect. Phys. Rev. Lett. **82**, 3112 (1999)

61. M. Saba, F. Quochi, C. Ciuti, D. Martin, J.-L. Staehli, B. Deveaud, A. Mura, G. Bongiovanni, Direct observation of the excitonic ac Stark splitting in a quantum well. Phys. Rev. B **62**, R16322 (2000)
62. S. Schmitt-Rink, D.S. Chemla, Collective excitations and the dynamical Stark effect in a coherently driven exciton system. Phys. Rev. Lett. **57**, 2752 (1986)
63. M. Combescot, R. Combescot, Excitonic Stark shift: A coupling to "semivirtual" biexcitons. Phys. Rev. Lett. **61**, 117 (1988)
64. S. Schmitt-Rink, D.S. Chemla, H. Haug, Nonequilibrium theory of the optical Stark effect and spectral hole burning in semiconductors. Phys. Rev. B **37**, 941 (1988)
65. C. Ell, J.F. Müller, K.E. Sayed, H. Haug, Influence of many-body interactions on the excitonic optical Stark effect. Phys. Rev. Lett. **62**, 304 (1989)
66. L. Quiroga, N.F. Johnson, Entangled Bell and Greenberger-Horne-Zeilinger states of excitons in coupled quantum dots. Phys. Rev. Lett. **83**, 2270 (1999)
67. B.W. Lovett, J.H. Reina, A. Nazir, G.A.D. Briggs, Optical schemes for quantum computation in quantum dot molecules. Phys. Rev. B **68**, 205319 (2003)
68. A. Nazir, B.W. Lovett, S.D. Barrett, J.H. Reina, G.A.D. Briggs, Anticrossings in Förster coupled quantum dots. Phys. Rev. B **71**, 045334 (2005)
69. C. Hettich, C. Schmitt, J. Zitzmann, S. Kuhn, I. Gerhardt, V. Sandoghdar, Nanometer resolution and coherent optical dipole coupling of two individual molecules. Science **298**, 385 (2002)
70. C. Hofmann, M. Ketelaars, M. Matsushita, H. Michel, T.J. Aartsma, J. Köhler, Single-molecule study of the electronic couplings in a circular array of molecules: Light-harvesting-2 complex from rhodospirillum molischianum. Phys. Rev. Lett. **90**, 013004 (2003)
71. R.H. Dicke, Coherence in spontaneous radiation processes. Phys. Rev. **93**, 99 (1954)
72. J.A. Leegwater, Coherent versus incoherent energy transfer and trapping in photosynthetic antenna complexes. J. Phys. Chem. **100**, 14403 (1996)